2D Magnetostatic Finite Element Simulation for Devices with a Radial Symmetry

Dries Vanoost[1,2], Herbert De Gersem[2,3], Joan Peuteman[1,4], Georges Gielen[5], Davy Pissoort[1,5]

[1]KU Leuven Kulab, ReMI Research Group, Oostende, Belgium
[2]KU Leuven Kulak, Wave Propagation and Signal Processing Research Group, Kortrijk, Belgium
[3]KU Leuven, Department of Physics and Astronomy, Solid-State Physics and Magnetism, Heverlee, Belgium
[4]KU Leuven, Department of Electrical Engineering, Electrical Energy and Computer Architecture, Heverlee, Belgium
[5]KU Leuven, Department of Electrical Engineering, Microelectronics and Sensors, Heverlee, Belgium

This paper proposes a two-dimensional magnetostatic finite-element solver for radially symmetric devices, complementary to the standard cartesian and axisymmetric solvers which are typically used for translatory and cylindrically symmetric configurations. In contrast to the cartesian and axisymmetric cases, a specific difficulty is encountered due to the particular dependence of the magnetic vector potential on the radial coordinate caused by the requirement for radial symmetry. Dedicated finite-element shape functions are developed such that the partition-of-unity property, consistency and convergence of the formulation are guaranteed. Implementation aspects and modelling pecularities are discussed. The new solver is validated for models for which analytical solutions exist. The modelling accuracy of the new 2D solver is compared to a 3D model for the calculation of the electromotive force and the electromagnetic torque of a twin-rotor axial-flux permanent-magnet synchronous machine.

***Index Terms*—Finite element methods, magnetostatics, convergence of numerical methods, partial differential equations, permanent magnet machines.**

I. Introduction

WHENEVER possible, 3D magnetic field simulation is avoided in favor of 2D simulation. This is possible when the geometry and the boundary conditions feature a translatory or cylindrical symmetry and the excitation currents are perpendicular to the symmetry plane, such that the magnetic flux lines lie in the plane of symmetry. Considering the magnetostatic formulation

$$\nabla \times (\nu \nabla \times \mathbf{A}) = \mathbf{J}_\mathrm{s} - \nabla \times \mathbf{H}_\mathrm{s} \tag{1}$$

with $\mathbf{A}$ the magnetic vector potential, ν the reluctivity, $\mathbf{J}_\mathrm{s}$ the applied current density and $\mathbf{H}_\mathrm{s}$ the source magnetic field strength of permanent-magnet (PM) material, in the cartesian and axisymmetric cases, $\mathbf{J}_\mathrm{s}$ and $\mathbf{A}$ have only z- or θ-components respectively, whereas $\mathbf{H}_\mathrm{s}$ and the magnetic flux density $\mathbf{B} = \nabla \times \mathbf{A}$ are confined to the perpendicular xy- or rz-plane. For the cartesian case, degrees of freedom (DoFs) are defined for the z-component of $\mathbf{A}$. The choice of DoFs for the cylindrical case is less obvious and was an item of discussion during the early nineties [14]. Eventually, a consensus arose on defining DoFs for $2\pi r A_\theta$ where A_θ is the θ-component of $\mathbf{A}$ [10]. It is advantageous to solve for flux linkages $\widehat{\mathbf{a}} = \ell_z A_z$ or $\widehat{\mathbf{a}} = 2\pi r A_\theta$ in unit Wb, because then, a generic implementation of the solver and the field-circuit coupling becomes possible [9], [7].

2D cartesian and axisymmetric solvers are standard, both in commercial software and freeware. Reductions to 2D for arbitrary symmetries have been proposed in e.g. [11], [18], [1]. Reductions for helical coordinates are reported in e.g. [15], [18], [1]. A 2D reduction of (1) for radial symmetry has not been proposed so far. This is remarkable because applications with a more or less radial symmetry exist (disk motors, cylindrical magnetic brakes, Fig. 1) and an appropriate 2D reduction seems straightforward [16]. In [2] and [20], axial-flux PM machines were represented by stacks of thin cylindrical shells (Fig. 1), each represented by a 2D cartesian model. This technique was organized as a workaround for dealing with radial instead of cartesian symmetry.

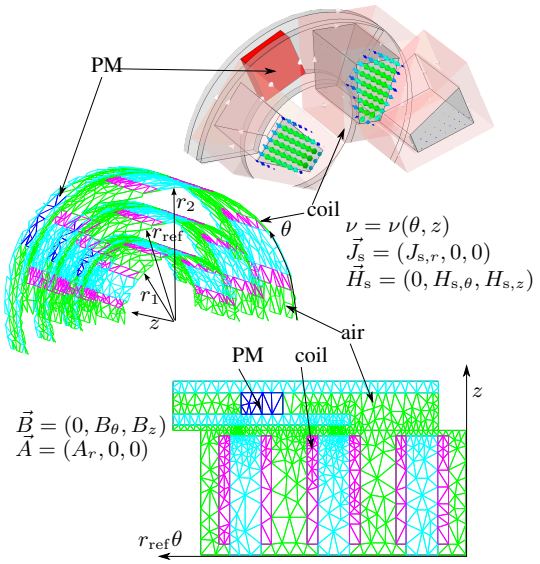

Fig. 1: Reduction of a 3D model of an axial-flux machine to a number of cylindrical shells, and further to a single stratified 2D model plane at which the 2D simulation is carried out.

In case of a symmetric geometry but non-symmetric excitations, the magnetic field is no longer symmetric. Nevertheless, when a smooth variation of the field along the direction of geometrical symmetry may be assumed, a *quasi-2D* solver may be the method of choice. The variation of the fields along the symmetry direction is represented by a small number of orthogonal functions, e.g., by harmonic functions in a study

Manuscript received XXX, XXXX. Corresponding author: Dries Vanoost (e-mail: dries.vanoost@kuleuven-kulak.be)
Digital Object Identifier inserted by IEEE

of machine end windings [3] or by Legendre polynomials in a study of a superconducting magnet system [12]. Couplings between 2D and 3D model parts have been proposed in e.g. [8]. In this paper, for the sake of conciseness, we restrict ourselves to a single model part featuring radial symmetry and to a linear magnetostatic formulation with isotropic materials. These restrictions can be alleviated easily but would need the introduction of a heavier notation which would hide the message of this paper.

Devices such as axial flux machines and cylindrical magnetic brakes have a more or less radially symmetric symmetry and carry magnetic flux lines confined in the θz-plane. Then, a promising reduction from 3D to 2D simulation consists of calculating $\mathbf{A} = (A_r(r,\theta,z), 0, 0)$ in a θz-plane. From this paper, it will become clear that this goal is not easily obtained. In contrast to the cartesian and axisymmetric cases, the unknown component $A_r(r,\theta,z)$ depends on all three spatial coordinates. Moreover, in analogy with the axisymmetric case, one should be careful when choosing FE shape functions. The remainder of the paper is organised as follows. Section II introduces the reduction to a 2D model, Section III develops an appropriate discretization, Section IV validates the approach, Section V address the peculiar behaviour for bending flux and Section VI discusses an application.

II. Reduction to Radial Symmetry

A cylindrical coordinate system (r,θ,z) with r the radial, θ the peripheral and z the axial coordinate is considered (Fig. 1). The model domain V reaches between $r_1(\theta,z)$ and $r_2(\theta,z)$ and has an arbitrary shape in the θz-plane. The model domain has a reluctivity ν, a current density $\mathbf{J}_\mathrm{s} = (h_\mathrm{j}/r, 0, 0)$ and a source magnetic field strength $\mathbf{H}_\mathrm{s} = (0, h_\theta/r, h_z)$ where ν, h_j, h_θ and h_z only depend on θ and z. The specific dependencies of $\mathbf{J}_\mathrm{s}$ and $\mathbf{H}_\mathrm{s}$ on r ensure the divergence-freeness of $\mathbf{J}_\mathrm{s}$ and the curl-freeness of $\mathbf{H}_\mathrm{s}$. A reference plane S_ref at reference radius r_ref is considered. For modeling convenience and visualization, the shell coordinates $(r_\mathrm{ref}\theta, z)$ are used (Fig. 1).

The assumptions allow to express (1) by

$$-\frac{1}{r}\frac{\partial}{\partial\theta}\left(\frac{\nu}{r}\frac{\partial A_r}{\partial\theta}\right) - \frac{\partial}{\partial z}\left(\nu\frac{\partial A_r}{\partial z}\right) = \frac{1}{r}\left(h_\mathrm{j} - \frac{\partial h_z}{\partial\theta} + \frac{\partial h_\theta}{\partial z}\right) \quad (2)$$

$$\frac{\partial}{\partial r}\left(\nu\frac{1}{r}\frac{\partial A_r}{\partial\theta}\right) = 0 \quad ; \quad (3)$$

$$\frac{1}{r}\frac{\partial}{\partial r}\left(r\nu\frac{\partial A_r}{\partial z}\right) = 0 \quad . \quad (4)$$

The additional equations (3) and (4) force the solution $A_r(r,\theta,z)$ to have a particular dependence on the radial coordinate r, i.e.,

$$A_r = r f(\theta) + \frac{1}{r} g(z) \quad , \quad (5)$$

where $f(\theta)$ only depends on θ and $g(z)$ only depends on z. The magnetic flux density is then $\mathbf{B} = (0, \frac{1}{r}\frac{\partial g}{\partial z}, -\frac{\partial f}{\partial\theta})$. The azimuthal and axial components of $\mathbf{B}$ have different dependencies on r. In a cylindrical setting, flux redistributing between θ- and z-directions requires a radial flux component, which is contradictory to the assumption of radial symmetry.

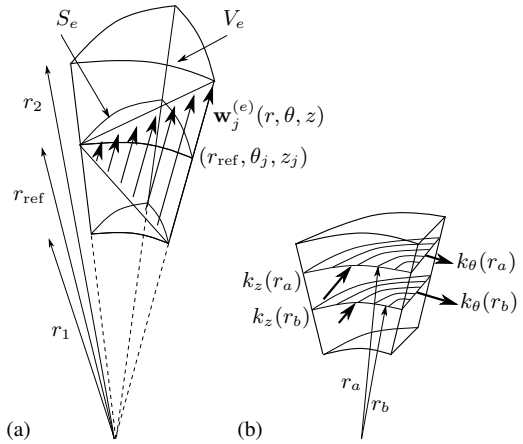

Fig. 2: (a) Edge shape function $\mathbf{w}_j^{(e)}(r,\theta,z)$ for element V_e constructed by extruding the bended triangle S_e from r_1 to r_2; (b) axial flux turning into azimuthal flux.

As a consequence, dealing with a bending flux in a 2D solver with radial symmetry necessarily comes together with an approximation.

III. Finite-Element Discretization

Formulation (2) needs to be discretized by edge shape functions that feature the particular dependence (5) on the radial coordinate r. An edge shape function $\mathbf{w}_j(r,\theta,z)$ is associated with a radial line through node (θ_j, z_j) (Fig. 2a). S_e is a triangle with straight edges in the θz-plane. An element $V_e = S_e \times [r_1, r_2]$ is constructed by extruding the triangle S_e from r_1 to r_2 while keeping the θ- and z-coordinates unchanged. In element V_e, $\mathbf{w}_j$ is expressed by

$$\mathbf{w}_j^{(e)}(r,\theta,z) = \frac{N_j^{(e)}(r,\theta,z)}{\ell_r}\mathbf{e}_r \quad ; \quad (6)$$

$$N_j^{(e)}(r,\theta,z) = \frac{a_j^{(e)}\frac{1}{r} + b_j^{(e)} r\theta + c_j^{(e)}\frac{1}{r}z}{2D_e} \quad . \quad (7)$$

Here, $\ell_r = r_2 - r_1$ is the extent of element V_e in radial direction, $N_j^{(e)}$ is a scalar function associated with node j and linearly decaying towards the other nodes of the element and $a_j^{(e)}$, $b_j^{(e)}$, $c_j^{(e)}$ and D_e are coefficients such that $N_j^{(e)}(r_\mathrm{ref},\theta_i,z_i) = \delta_{ij}$. The constructed shape functions fulfill the following properties:

- *partition-of-unity*: the integration of $\mathbf{w}_j$ along a radial line through the associated node j yields 1, whereas integration along a radial line through any other node yields 0 [4].
- *consistency*: the set of edge shape functions are able to represent a homogeneous axial field and an azimuthal field with dependence $1/r$ exactly.
- *convergence*: the set of edge shape functions approximates a field distribution with a discretization error of order $\mathcal{O}(h^2)$ where h denotes the mesh size.

Formulation (2) is discretized by the Ritz-Galerkin approach, using $\mathbf{w}_j(r,\theta,z)$ both as test and trial functions, leading to the system of equations

$$\mathbf{K}_\nu \widehat{\mathbf{a}} = \widehat{\mathbf{j}}_\mathrm{s} + \widehat{\mathbf{j}}_\mathrm{pm} \quad (8)$$

where

$$\mathbf{K}_{\nu,ij} = \int_V (\nu\nabla\times\mathbf{w}_i)\cdot(\nabla\times\mathbf{w}_j)\,\mathrm{d}V \quad ; \tag{9}$$

$$\hat{\mathbf{j}}_{\mathrm{s},i} = \int_V \mathbf{J}_\mathrm{s}\cdot\mathbf{w}_i\,\mathrm{d}V \quad ; \tag{10}$$

$$\hat{\mathbf{j}}_{\mathrm{pm},i} = -\int_V \mathbf{H}_\mathrm{s}\cdot(\nabla\times\mathbf{w}_i)\,\mathrm{d}V \quad . \tag{11}$$

Substituting (6) and (7) and integrating for a single element V_e leads to elementary 3-by-3 matrices $\mathbf{K}_\nu^{(e)}$ and elementary 3-by-1 vectors $\hat{\mathbf{j}}_\mathrm{s}^{(e)}$ and $\hat{\mathbf{j}}_\mathrm{pm}^{(e)}$ to be assembled into $\mathbf{K}_\nu$, $\hat{\mathbf{j}}_\mathrm{s}$ and $\hat{\mathbf{j}}_\mathrm{pm}$ by the standard FE procedure:

$$\mathbf{K}_{\nu,ij}^{(e)} = \frac{c_i^{(e)}\nu c_j^{(e)}\chi + b_i^{(e)}\nu b_j^{(e)}\gamma}{4D_e\ell_r} \quad ; \tag{12}$$

$$\hat{\mathbf{j}}_{\mathrm{s},i}^{(e)} = \frac{D_e}{3r_\mathrm{ref}}h_\mathrm{j} \quad ; \tag{13}$$

$$\hat{\mathbf{j}}_{\mathrm{pm},i}^{(e)} = -\frac{h_\theta c_i^{(e)}}{2}\chi + \frac{h_z b_i^{(e)}}{2}\gamma \quad , \tag{14}$$

where $\chi = \frac{\ln r_2 - \ln r_1}{\ell_r r_\mathrm{ref}}$, $\gamma = \frac{r_\mathrm{m}}{r_\mathrm{ref}}$ and $r_\mathrm{m} = \frac{r_1+r_2}{2}$ are element-wise adaptation factors calculated for the average inner and outer radii of the considered element. The choice $r_\mathrm{ref} = r_\mathrm{m}$ substantially simplifies the expressions for $a_j^{(e)}$, $b_j^{(e)}$, $c_j^{(e)}$, D_e, $\mathbf{K}_{\nu,ij}^{(e)}$ and $\hat{\mathbf{j}}_{\mathrm{pm},i}^{(e)}$, and is applied in the implementation. After introducing the boundary conditions, the algebraic system (8) is sparse, symmetric and positive definite and can be solved by a sparse direct solver or by a preconditioned conjugate gradient method [19].

IV. Consistency and Convergence Check

The consistency and convergence of the discretization is verified for four analytical models that have an extent $[r_1, r_2]\times[0,\theta_2]\times[0,z_2]$, are filled with homogeneous material and are submitted to four different excitations (Fig. 3). They have an excitation of respectively:

- a homogeneous axial flux ϕ_ax exerted by the boundary conditions $\hat{\mathbf{a}}(0,z) = 0$ and $\hat{\mathbf{a}}(\theta_2,z) = \phi_\mathrm{ax}$;
- an azimuthal flux ϕ_az exerted by the boundary conditions $\hat{\mathbf{a}}(\theta,0) = 0$ and $\hat{\mathbf{a}}(\theta,z_2) = \phi_\mathrm{az}$;
- an axial flux exerted by a radial current density $J_r = \frac{1}{r}\frac{I_\mathrm{app}}{\theta_2 z_2}$ with I_app the applied current;
- a flux exerted by a permanent magnet with remanence B_r at the reference plane and a magnetization angle φ with respect to the azimuthal direction.

The discretization error converges to machine precision for the models with homogeneous axial flux and curl-free azimuthal flux (Fig. 4). This illustrates the consistency of the FE shape functions [5]. For the other analytic test cases, the convergence of the discretization error is order $\mathcal{O}(h^2) = \mathcal{O}(n^{-1})$ with h the mesh size and n the number of DoFs, which is the expected convergence order for linear FE shape functions [5]. These checks validate the particular choice of the FE shape functions. Other choices, e.g. with other dependencies on r, will typically fail in these tests.

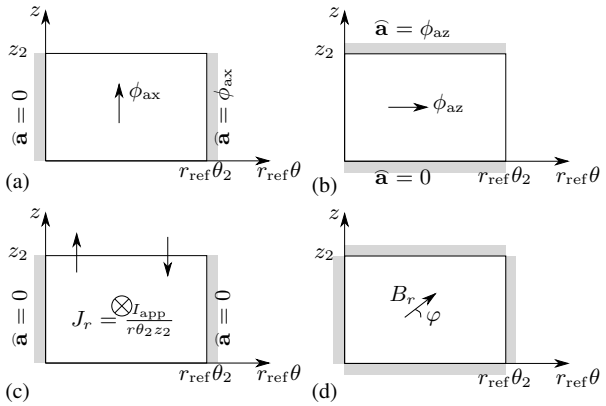

Fig. 3: Analytical models for consistency and convergence checks and their solutions: (a) with impressed axial flux ($A_r = -\frac{\phi_\mathrm{ax}}{S_\mathrm{ax}}r\theta$); (b) with impressed azimuthal flux ($A_r = -\frac{\phi_\mathrm{az}}{r\ln\frac{r_2}{r_1}}\frac{z}{z_2}$); (c) axial flux generated by a radial current ($A_r = \frac{\mu I_\mathrm{app}}{\theta_2 z_2}\frac{r\theta}{2}(\theta_2-\theta)$); (d) PM material ($A_r = \frac{r_\mathrm{ref}}{r}B_r z\cos\varphi - B_r r\theta\sin\varphi + \alpha\left(r\theta^2 - \frac{z^2}{r}\right)$).

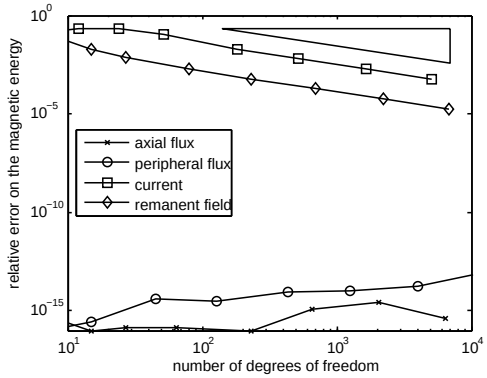

Fig. 4: Convergence of the discretization error of formulation (1), discretization by the radially symmetry edge shape functions (6).

V. Bending Flux

Because the azimuthal and axial components of $\mathbf{B}$ have different dependences on r, the reduced formulation is not capable of representing a bended magnetic field. In Fig. 2b, $k_z(r)$ denotes the line flux density (in Wb/m) entering the considered volume at a radius r in the axial direction, whereas $k_\theta(r)$ denotes the line flux density leaving the volume in azimuthal direction. These line flux densities depend on r as $k_z \sim r$ and $k_\theta \sim \frac{1}{r}$. As a consequence when the line flux density is conserved at a shell at radius r_a, i.e., $k_z(r_a) = k_\theta(r_a)$, then this is no longer true for the shell at another radius r_b. This inconsistency of the continuous formulation (2) is, however, alleviated by the discretization procedure. The DoFs $\hat{\mathbf{a}}$ attribute fluxes to the radial lines perpendicular to the nodes of the 2D model. This guarantees that all flux entering an element V_e through one of its faces leaves the element through one of its other faces. Any necessary redistribution of axial flux components into azimuthal flux components or vice versa is possible by radial components inside V_e experiencing a zero reluctivity in the radial direction. The fourth analytical example deals with a bending flux and shows a second order convergence for the discretization error.

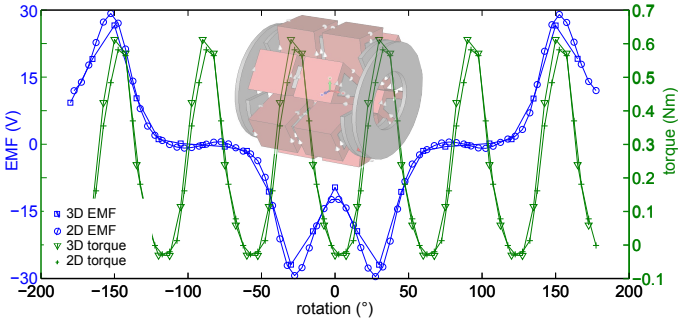

Fig. 5: Electromotive force and electromagnetic torque generated by the twin-rotor axial-flux permanent-magnet synchronous machine at 3000 rpm.

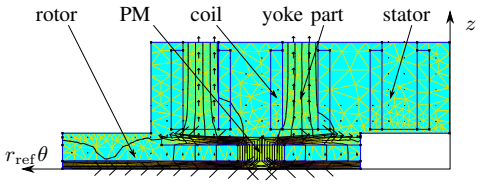

Fig. 6: Magnetic flux lines at a θz-shell at $r = r_{\mathrm{ref}}$.

VI. Application

The 2D FE solver for radially symmetric models is applied to calculate the performance of a three-phase twin-rotor axial-flux PM synchronous machine (Fig. 1) [17]. The stator consists of twelve coils wound around six iron yoke parts attached to a back-iron disk. The rotors, one at the front and the other at the back of the stator, each consist of two PMs attached to each other one in the middle of the machine with a non-magnetic material. The two rotors are π radians shifted such that the opposite magnetic poles are across each other. A 2D model with 6800 DoFs is constructed using FEMM [13] and simulated by the newly developed FE solver implemented in MATLAB. A reference 3D model with 200000 DoFs is constructed and simulated using CST EMStudio [6]. The no-load electromotive force is post-processed from the solution for $\widehat{\mathbf{a}}$. The electromagnetic torque is derived from the magnetic co-energy. The 2D reduction introduces severe approximations: flux fringing at the inner and outer ends is neglected, as it is the case for any 2D model; PM cubes are approximated by ring segments (with the same remanent flux); bending magnetic fluxes are assumed to redistribute along radial paths with zero reluctivity inside the FEs. Nevertheless, the 2D solver for radially symmetric models achieves acceptable results. The 2D results for the electromotive force and the electromagnetic torque differ by 5.50% and 8.50% respectively from their 3D counterparts. These differences are fully attributed to the 2D modelling assumptions. The 2D solver is valuable for fast determination of major machine parameters during initial design steps. The magnetic flux lines are visualized on the θz-shell at $r = r_{\mathrm{ref}}$ (Fig. 6).

VII. Conclusion

The components of a radially symmetric magnetic flux density have specific dependencies on the radial coordinate. A 2D formulation in terms of the radial component of the magnetic vector potential needs to be discretized using edge shape functions that support these dependencies. At the continuous level, the 2D reduction does not allow exchange of axial and azimuthal flux components. In the discrete setting, however, bending fluxes becomes possible because a radial field component may exist at the inner element level. Such particular behavior is not encountered for cartesian and axisymmetric 2D reductions. 2D simulations for a three-phase twin-rotor axial-flux PM synchronous machine give accurate results.

Acknowledgements

This doctoral research is funded by the "Agency for Innovation by Science and Technology in Flanders (IWT)" and by the grant KUL_3E100118 "Electromagnetic field simulation for future particle accelerators".

References

[1] B. Auchmann, B. Flemisch, and S. Kurz. A discrete 2-D formulation for 3-D field problems with continuous symmetry. *IEEE Trans. Magn.*, 46(8):3508–3511, Aug. 2010.

[2] J. Azzouzi, G. Barakat, and B. Dakyo. Quasi-3-D analytical modelling of the magnetic field of an axial flux permanent-magnet synchronous machine. *IEEE Trans. Energy Convers.*, 20(4):746–752, 2005.

[3] G. Bedrosian, M. Chari, A. deBlois, M. Palmo, M. Shah, and G. Theodossiou. Axiperiodic finite element analysis of generator end regions, part II - application. *IEEE Trans. Magn.*, 25(4):3070–3072, July 1989.

[4] A. Bossavit. *Computational Electromagnetism, Variational formulations, Edge elements, Complementarity*. Academic Press, Boston, 1998.

[5] P. Ciarlet. *The Finite Element Method for Elliptic Problems*. Number 4 in Studies in mathematics and its applications. North-Holland Amsterdam, 1978.

[6] Computer Simulation Technology AG. CST EM Studio. www.cst.com.

[7] H. De Gersem, K. Hameyer, and T. Weiland. Field-circuit coupled models in electromagnetic simulation. *J. Comput. Appl. Math.*, 168(1-2):125–133, July 2004.

[8] H. De Gersem, S. Koch, and T. Weiland. Accounting for end effects when calculating eddy currents in thin conductive beam tubes. *IEEE Trans. Magn.*, 45(3):1040–1043, Mar. 2009.

[9] J. Gyselinck. *Twee-dimensionale dynamische eindige-elementenmodellering van statische en roterende elektromagnetische energieomzetters*. PhD thesis, Universiteit Gent, Mar. 2000.

[10] F. Henrotte, H. Hedia, N. Bamps, A. Genon, A. Nicolet, and W. Legros. A new method for axisymmetrical linear and nonlinear problems. *IEEE Trans. Magn.*, 29(2):1352–1355, Mar. 1993.

[11] F. Henrotte, B. Meys, H. Hedia, P. Dular, and W. Legros. Finite element modelling with transformation techniques. *IEEE Trans. Magn.*, 35(3):1434–1437, May 1999.

[12] S. Koch, H. De Gersem, and T. Weiland. Hybrid finite-element, spectral-element discretization for translatory symmetric model parts. *IEEE Trans. Magn.*, 44(6):722–725, June 2008.

[13] D. Meeker. Finite element method magnetics (FEMM). www.femm.info/wiki/HomePage.

[14] J. Melissen and J. Simkin. A new coordinate transform for the finite element solution of axisymmetric problems in magnetostatics. *IEEE Trans. Magn.*, 26(2):391–394, Mar. 1990.

[15] A. Nicolet, A. B. Movchan, S. Guenneau, and F. Zolla. Asymptotic modelling of weakly twisted electrostatic problems. *C.R. Mecanique*, 334:91–97, 2006.

[16] O. Niemimäki. *Improved quasi 3D modelling and simulation of axial flux machines*. Msc thesis, Tampere University of Technology, 2012.

[17] A. Parviainen, M. Niemelä, and J. Pyrhönen. Modeling of axial permanent-magnet machines. *IEEE Trans. Ind. Appl.*, 40(5):1333–1340, September/October 2004.

[18] P. Raumonen, S. Suuriniemi, T. Tarhasaari, and L. Kettunen. Dimensional reduction in electromagnetic boundary value problems. *IEEE Trans. Magn.*, 44(6):1146–1149, June 2008.

[19] Y. Saad. *Iterative Methods for Sparse Linear Systems*. PWS Publishing Company, Boston, 1996.

[20] H. Vansompel, P. Sergeant, and L. Dupré. A multilayer 2-D–2-D coupled model for eddy current calculation in the rotor of an axial-flux PM machine. *IEEE Trans. Energy Convers.*, 27(3):784–791, Sept. 2012.